NUCLEAR STRUCTURE AT PARTICLE DRIP LINES*

J. DOBACZEWSKI[a,b], I. HAMAMOTO[a,c], W. NAZAREWICZ[a,b,d,e]

AND J.A. SHEIKH[a,f]

[a]Joint Institute for Heavy Ion Research
Oak Ridge National Laboratory, Oak Ridge, TN 37831, U.S.A.

[b]Institute of Theoretical Physics, Warsaw University
Hoża 69, PL-00-681, Warsaw, Poland

[c]Department of Mathematical Physics, Lund Institute of Technology
S-22100 Lund, Sweden

[d]Physics Division, Oak Ridge National Laboratory
Oak Ridge, TN 37831, U.S.A.

[e]Department of Physics, University of Tennessee
Knoxville, TN 37996, U.S.A.

[f]Tata Institute of Fundamental Research
Colaba, Bombay-400 005, India

(Received October 30, 1993)

Several examples of mean-field calculations, relevant to the recent and planned low-spin experimental works, are presented. The perspectives for future studies (mainly related to spectroscopy of exotic nuclei) are reviewed.

PACS numbers: 21.10. Dr, 21.10. Ft, 21.10. Pc, 21.60. Jz

1. Introduction

There are some substantial new challenges that confront the nuclear physics community. The common denominator for those challenges is *nuclear physics at extreme conditions.* One of such new avenues is nuclear

* Presented at the XXIII Mazurian Lakes Summer School on Nuclear Physics, Piaski, Poland, August 18–28, 1993.

physics at very high angular momenta. The recently constructed new-generation multidetector arrays (*e.g.*, EUROGAM, GAMMASPHERE, GA.SP) will enable us to study discrete nuclear states up to the fission limit as well as a high-spin, high-T quasi-continuum. The second direction is represented by the new relativistic heavy-ion facilities (*e.g.*, RHIC). Here, researches hope to investigate the ways the atomic nucleus behaves and rearranges itself at extreme energies, densities, and pressure. The third avenue will take us to the *terra incognita* of extreme isospins. Experimentally, such an excursion will be possible thanks to new efforts to produce radioactive heavy ion beams. This new departure promises a view of nuclear structure in previously unexplored areas far from stability, and heralds a new era of increased cooperation between the fields of nuclear physics and astrophysics.

From the theoretical point of view, spectroscopy of exotic nuclei offers a unique test of those components of effective interactions that depend on isospin degrees of freedom. In this paper, several aspects of nuclear structure at the limits of extreme isospin, *i.e.*, at particle drip lines, are discussed by means of the mean-field approach and its extensions. In Section 2, self-consistent approaches, namely Hartree-Fock (HF), Hartree-Fock-Bogolyubov (HFB), and Relativistic Mean Field (RMF), are used to make predictions for the spherical shell structure of exotic drip-line nuclei. Section 3 contains selected results of calculations for nuclei around doubly-magic ^{100}Sn. The calculations based on quasiparticle random phase approximation (QRPA) for low-energy isovector 1^+ states in N$\sim$Z nuclei are presented in Section 4.

2. Spherical shell structure at particle drip lines

Theoretically, the physics of radioactive ion beams is a challenge for well established models of nuclear structure and, because of dramatic extrapolations involved, it invites a variety of theoretical approaches. Since the parameters of interactions used in the usual mean-field calculations, such as the Skyrme interaction in the HF approach, are determined so as to reproduce the properties of beta-stable nuclei, the parameters may not always be proper to be used in the calculation of drip-line nuclei. In fact, because of the sensitivity of the single-particle spectrum to theoretical details (*e.g.*, choice of effective interaction, treatment of exchange terms, *etc.*) predicted drip lines are strongly model-dependent [1–5].

Recently, the global properties of shell structure of drip-line nuclei have been discussed [6] by means of three state-of-the-art mean-field models, namely the HF and the HFB models with Skyrme-type interactions (SkP, SIII, SkM*), and the RMF model with the NL1 and NL-SH forces. In order to analyze the trends towards drip-line nuclei, the isobaric chains of nuclei with a constant A were investigated.

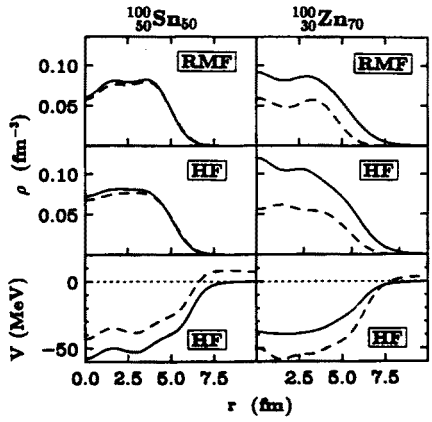

Fig. 1. Single-particle nucleonic densities of the NL1 RMF model for the A=100 drip-line nuclei, ^{100}Sn and ^{100}Zn (neutrons: solid line, protons: dashed line). Middle (bottom): corresponding single-particle densities (central potentials) of the SkP HF approach.

The extreme situation expected at the A=100 drip lines is displayed in Fig. 1 for the proton-drip-line nucleus $^{100}_{50}Sn_{50}$ and the neutron-drip-line nucleus $^{100}_{30}Zn_{70}$. Shown here are the self-consistent proton and neutron densities, and the central potentials (plus the Coulomb potential for protons). It is seen that the densities calculated in the HF and RMF models are fairly similar. A striking feature seen in the neutron-drip-line nucleus ^{100}Zn is the presence of a large diffuseness in the neutron density as well as in the proton potential. According to the calculations of Ref. [6], for a given isobaric sequence the effective HF and RMF diffuseness of neutron densities are very similar; they increase dramatically when approaching the neutron-drip-line nuclei. On the other hand, the neutron radius parameter shows weak variations with neutron number.

The RMF single-particle energies for the $A = 100$ and $A = 150$ isobars are plotted as a function of N in Fig. 2. As a result of the truncated oscillator basis the calculated single-particle levels with positive energies (continuum) are discrete. The results obtained in the HF model are very similar (the positive-energy discrete states in HF are due to the finite radius of the box in which the HF equations were solved). In both calculations it is seen that the bulk single-particle shell structure exhibited by bunching of bound levels and the presence of magic gaps at particle numbers 50, 82, and 126 does not appreciably change as one approaches the neutron-drip-line. The positive-energy low-j continuum manifests itself through the presence of many levels which practically do not vary as a function of N. Indeed, since those states are not localized inside the nuclear volume their dependence on details of the average potential is expected to be very weak (a weak Z-dependence of

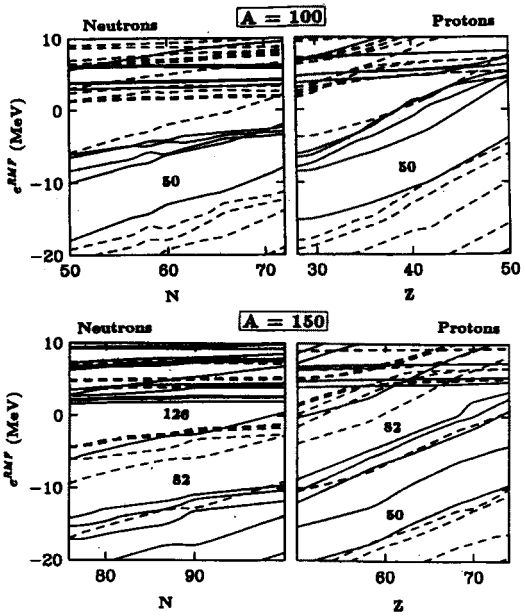

Fig. 2. Spherical single-particle levels for the A=100 and 150 isobars calculated in the RMF model with the NL-SH interaction [7] as a function of neutron and proton number. Solid (dashed) lines represent the orbitals with positive (negative) parity.

proton continuum results from the change in Coulomb potential). It is also seen that the combined effect of centrifugal and Coulomb forces gives rise to positive-energy states which try to preserve their shell structure. Those can be interpreted as quasi-bound resonances, especially pronounced for protons (for reference: the Coulomb barrier in ^{100}Sn is about 9 MeV).

The neutron-number dependence of the NL-SH RMF single-particle density for ^{100}Sn (proton drip-line system), ^{118}Sn (stable), ^{132}Sn (neutron-rich), and ^{150}Sn (neutron drip-line system) is displayed in Fig. 3. Apart from the density fluctuation in the nuclear interior coming from the detailed nuclear shell-structure, the average neutron density in the interior stays fairly constant, while the proton density decreases as the neutron number increases. However, the ratio of the neutron to the proton density in the interior does not increase as fast as the ratio N/Z. This, together with the fact that the neutron radius increases faster than the proton radius, develops the neutron skin at the surface of nuclei with a large neutron excess. Note also the increase of the neutron surface-diffuseness, which is clearly seen as the neutron drip-line is approached.

The pairing force may have a unique role in drip-line nuclei due to the scattering of nucleonic pairs from bound states to positive-energy orbitals.

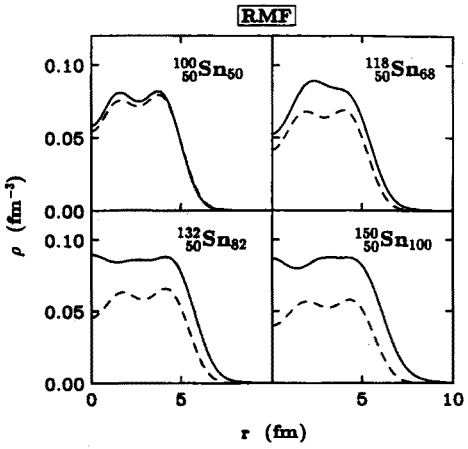

Fig. 3. Single-particle nucleonic densities of the NL-SH RMF model for ^{100,118,132,150}Sn isotopes (neutrons: solid line, protons: dashed line).

In the HF model with the state-independent seniority pairing this leads to the presence of unphysical "particle gas" surrounding the nucleus [8]. This problem is overcome in the HFB method with a realistic pairing interaction in which the coupling of bound states to continuum is correctly taken into account [8]. In order to describe the coupling between bound states and continuum due to pairing, the HFB calculations with the SkP force have been performed [6]. Figure 4 shows the expectation values $\varepsilon_k = \langle \Psi_k | h | \Psi_k \rangle$ of the single-particle Hamiltonian, $h = \delta E_{\rm HFB}/\delta\rho$ [9], in the canonical basis for the $A = 120$ and $A = 150$ isobars. As argued in Ref. [6], *(i)* the single-particle canonical energies, ε_k, carry most information on the shell energy and *(ii)* the low-lying quasiparticle excitations and proton and neutron separation energies, $S \simeq \lambda + E_k$, are governed by ε_k's. For the isobaric chain of $A = 120$, the neutron Fermi energy approaches zero near $N = 82$. As seen in Fig. 4 (top), the $N = 82$ shell gap dramatically decreases near the neutron-drip line. This effect is primarily caused by a lowering of single-particle (canonical) energies of low-j orbitals relative to those of high-j orbitals. Such an effect results from a strong interaction between bound orbitals and the low-j continuum, whereas the interaction with high-j resonance states is much less effective in modifying bound orbitals. For heavier systems with $N > 82$ there are more high-j orbitals in major shells and the lowering of low-j subshells (which, in addition, are located at the top of shells) is not sufficient to close the gaps completely. This is illustrated in Fig. 4 (bottom) for the $A = 150$ isobars. Indeed, the shell structure at $N \sim 100$ is very weakly affected as compared to the $A = 120$ case. According to calculations, the disappearance of shell effects at the neutron-drip line is only expected in the systems with $N \leq 82$. At the proton-drip line, the quenching occurs only

for light systems with $Z \leq 28$, because the Coulomb barrier prevents the low-j continuum from approaching bound states. A quenching of this type has recently been demonstrated by the SkP HFB calculations of spherical drip lines [4].

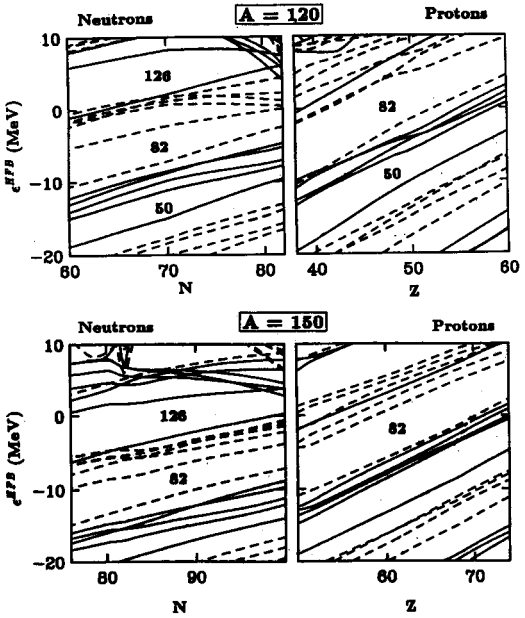

Fig. 4. Spherical single-particle levels for the $A = 120$ and 150 isobars calculated in the SkP HFB model as a function of neutron number. The single-particle canonical HFB energies are given by $\varepsilon_k = \langle \Psi_k | h | \Psi_k \rangle$. Solid (dashed) lines represent the orbitals with positive (negative) parity.

As discussed above, the diffuseness of the one-body neutron potential becomes larger as the neutron drip-line is approached. Consequently, the shape of the potential becomes more similar to that of an oscillator potential, see Fig. 1, and the neutron single-particle spectrum for systems with large neutron excess can be well approximated by that of the Nilsson model without the l^2 term [6].

3. ^{100}Sn — a Holy Grail

The study of properties of heavy doubly-magic nuclei and neighboring systems is a very important testing ground for the ability of the existing models to describe and predict the underlying shell structure. Until recent years, the nucleus ^{208}Pb was the only heavy doubly-magic nucleus with the experimentally known binding energies of the valence single-particle

states. On the neutron-rich side, there has been a considerable amount of data collected for the doubly-magic ^{132}Sn. The proton-rich doubly-magic ^{100}Sn is expected to lie just on the border of the proton drip line. In the previous work by Leander *et al.* [10] the observed single-particle energies in ^{132}Sn were compared with the Hartree–Fock model with the SIII interaction, the folded-Yukawa single-particle potential, and the Woods–Saxon potential. The results of the calculations are presented in Fig. 5. The parts (a) and (b) show how the center of gravity of a set of single-particle energies deviates from experiment in the Woods-Saxon, folded-Yukawa, and SIII models. As noticed by Blomqvist [11], there is a correspondence between ^{132}Sn and ^{208}Pb: for each level (n,l,j) in ^{132}Sn there is a corresponding level $(n,l{+}1,j{+}1)$ in ^{208}Pb. As seen in Fig. 5 the deviations in ^{132}Sn and ^{208}Pb mostly go together, *i.e.*, the single-particle levels in both nuclei are similar. For the nucleus ^{100}Sn the corresponding structural analog is expected to be ^{56}Ni. The lower part (c) of Fig. 5 shows the binding energy of the $1g_{9/2}$ proton in ^{100}Sn and the $1f_{7/2}$ shell in ^{56}Ni. If the deviations from experiment go together in these two nuclei, ^{100}Sn would be stable with respect to proton emission, with a proton binding energy of about 3 MeV. This binding energy is relatively favorable for synthesis of this doubly-magic nuclide, although, for example, neighboring ^{101}Sb would be proton unstable. The above analysis of shell structure in ^{100}Sn emphasizes the importance of using several different models when extrapolating their results far from stability.

One can attempt to approach ^{100}Sn by systematic studies of neighboring nuclei. In this region, one of the most important pieces of information are the properties of the Gamow-Teller (GT) decay of even nuclei. Selected properties of the GT beta decay of even nuclei near ^{100}Sn have been studied in Ref. [12] within two theoretical models: a self-consistent HFB approach with the SkP interaction (Model I) and the shell correction method with the Woods-Saxon average potential and the monopole pairing interaction (Model II). Figure 6 shows the comparison of the calculated and experimental electron-capture decay energies Q_{EC} (*i.e.*, differences between atomic masses of nuclei in their ground states) for the even-even parent nuclei near ^{100}Sn. The upper portion shows the results of calculations under the assumption of spherical shape for both the parent and daughter nuclei. To see the influence of deformation-polarisation effects the condition of spherical shape was relaxed in the Model II, see Fig. 6, lower portion. The deformed calculations nicely reproduce the experimental ground-state deformations and spins of $^{104-110}$In. The inclusion of deformation essentially improves the agreement between results of the Model II and the experimental data: the calculated $Q_{\rm EC}$ values are remarkably close to the measured ones. The calculated shapes of the odd-odd nuclei in the 1^+ excited $(\pi g_{9/2}^{-1} \otimes \nu g_{7/2})$

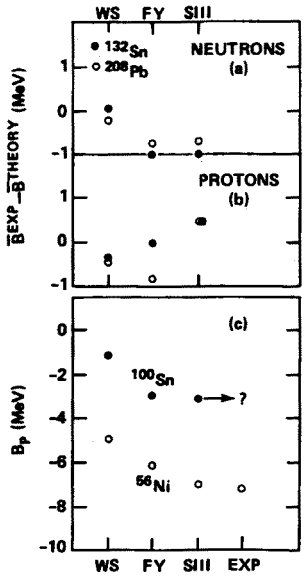

Fig. 5. Deviation between experimental and theoretical center of gravity of a set of single-particle levels in the Woods-Saxon, folded Yukawa, and SIII HF models for ^{132}Sn and ^{208}Pb (top). The bottom part shows the binding energy of the $1g_{9/2}$ proton shell in ^{100}Sn and the $1f_{7/2}$ shell in ^{56}Ni.

states turned out to be spherical. This suggests that the deformation of the daughter nucleus may be significant for an estimate of the $Q_{\rm EC}$ values while it may be less important for the GT transition energy. The obtained good agreement with experimental data makes it possible to give a fairly precise estimate for $Q_{\rm EC}$ values for not yet studied nuclei. Calculations predicted $Q_{\rm EC}$ values of 5.5 MeV and 7.8 MeV for ^{98}Cd and ^{100}Sn, respectively. The recent data from GSI for ^{98}Cd support this theoretical prediction; the estimated [13] value of $Q_{\rm EC}$ ~5.33 MeV is indeed very close to the calculated one. The estimated GT hindrance factor turned out to be about 6.5, *i.e.*, very similar to that found in the $\pi h_{11/2} \rightarrow \nu h_{9/2}$ decays in the rare earth region. Here we note that the GT (ΔZ=−1) giant resonance, which contains the major part of the possible GT strength, is estimated to lie energetically well below the ground state of ^{100}Sn and, thus, can be reached also by GT beta decay [14]. For the recent calculations around ^{100}Sn, see Refs [15–20].

4. Low-lying 1^+ states in the medium-mass N=Z nuclei

Spectroscopy of nuclei with $T_z \lesssim 0$ will become one of the main arenas of investigations around the proton drip line. Experimentally, shape coexistence, large deformations, quenching of pairing correlations, and dramatic

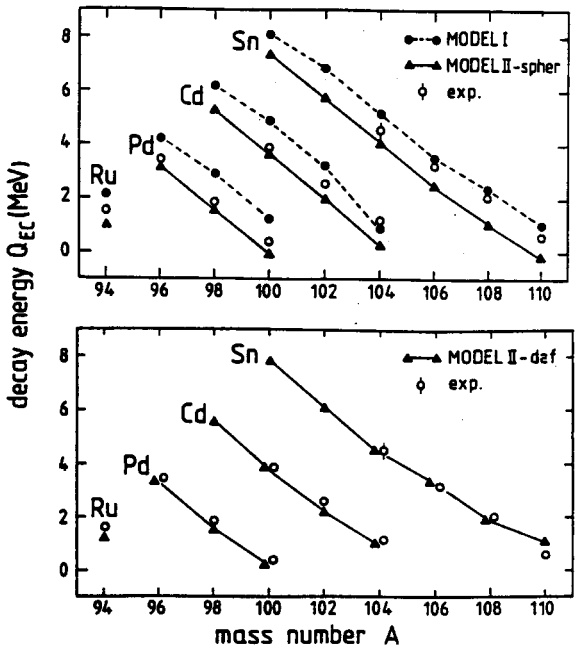

Fig. 6. Calculated and experimental Q_{EC} values for the even-even parent nuclei near ^{100}Sn.

shape changes induced by rotation are quite common phenomena in the zirconium region ($Z \simeq N \simeq 40$). The microscopic reason for such a strong variation of collective properties is the low single-particle level density in these medium-mass nuclei. In the $A \sim 80$ region both protons and neutrons lie in the same $(p_{1/2}, p_{3/2}, f_{5/2}, g_{9/2})$ shell. For $T_z \sim 0$ systems, the proton and neutron shell corrections add coherently. A beautiful experimental signature of large prolate deformations in the $A \sim 80$ region, attributed to the prominent shell-structure at $Z, N = 38$ and 40, was the observation of very collective rotational bands in neutron-deficient Sr and Zr isotopes [21–23]. Because of spectacular shape effects, relatively small size, and high collectivity, the nuclei from the $A \sim 80$ mass region have become favorite testing grounds for various theoretical approaches. Calculations based on the mean-field approach applied to nuclei in the light-Zr region suggest an interpretation of experimental data in terms of well-deformed prolate shapes, weakly-deformed oblate shapes, and spherical (shell-model) configurations [24–26].

Since the $M1$ collectivity of low-lying 1^+ states increases with deformation, it is anticipated that in some well deformed nuclei in the $A \sim 80$ mass region the strong magnetic dipole strength should be concentrated at low energies. In the $A \sim 80$ mass region there are several good examples of very

regular, rigid rotational bands. Theoretically, they are associated with two-quasiparticle excitations built upon the proton [431 3/2]⊗[312 3/2] Nilsson orbitals which happen to occur just below the strongly deformed subshell closure at $Z = 38$. The BCS calculations [27] suggest the dramatic reduction (or collapse) of the static pairing in these configurations; this has important consequences for the low-energy electromagnetic transitions. Since the $B(M1)$ values involving the ground state of even-even nuclei are proportional to the BCS factor $(u_\mu v_\nu - v_\mu u_\nu)^2$, weaker pair correlations lead to a stronger low-lying $M1$ strength.

The deformation dependence of 1^+ states is a current subject of both experimental [28, 29] and theoretical [30–33] studies. The low-energy $B(M1)$ strength (defined as the summed strength up till excitation energies of about 4 MeV) increases with quadrupole deformation as, roughly, β_2^2. Many of the $A \sim 80$ nuclei are very well deformed in their ground states, their equilibrium deformations exhibit rapid isotopic and isotonic variations, and their pairing correlations are expected to be weak due to deformed subshell closures. Because the Kr, Sr, and Zr isotopes have these characteristics, they are ideally suited for investigations of the low-energy $M1$ strength and its deformation dependence.

The properties of the $K^\pi = 1^+$ states have been investigated [34] using the QRPA Hamiltonian of Ref. [35] containing the single-particle Woods–Saxon field, the monopole-pairing field, a long-ranged residual interaction (mainly of quadrupole–quadrupole type), and the spin-spin residual interaction. As a representative example, results of calculations for Sr isotopes are presented in Fig. 7 which shows the excitation energies of the low-lying $K^\pi = 1^+$ states. The values $B(M1; g.s \rightarrow 1^+)$ (in μ_N^2) are indicated. The upper diagram was obtained by using the standard pairing gaps. According to calculations, pairing correlations in the excited states of Sr-Zr are expected to be seriously quenched. Therefore, we performed a second set of calculations with Δ_p and Δ_n reduced by 50% with respect to the standard values. As expected and seen in Fig. 7, the $B(M1)$ values calculated in the "weak pairing" variant are approximately twice as large as the $M1$ rates obtained in the "standard pairing" variant.

The best candidate for low-lying enhanced 1^+ states in the $A \sim 80$ mass region is the $N = Z$ nucleus ^{76}Sr. In both pairing variants of calculations, there appears only one low-lying 1^+ state which has unusually strong $M1$ collectivity. In the "weak pairing" variant this state is predicted at 2.2 MeV and the corresponding $B(M1; g.s. \rightarrow 1^+)$ transition is 2.16 μ_N^2. The main components of the wave function of the 1^+ state in ^{76}Sr are the $\pi(g_{9/2})^2$ and $\nu(g_{9/2})^2$ excitations involving the two Nilsson orbitals [431 3/2] and [422 5/2].

The contribution to the $B(M1)$ strength coming from the unique-parity

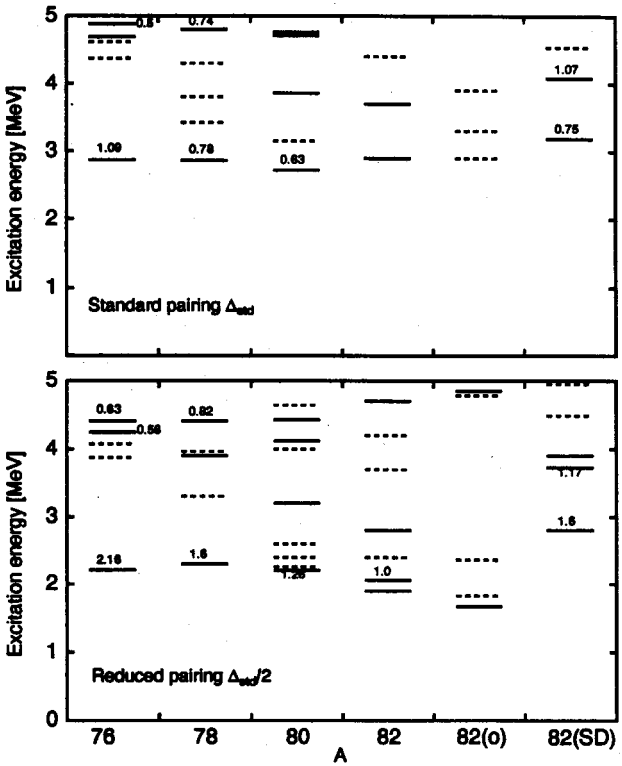

Fig. 7. Predicted excitation energies of low-lying 1^+ states of prolate configurations in ^{76,78,80,82}Sr, oblate minimum in ^{82}Sr [82(o)], and the superdeformed configuration in ^{82}Sr [82(SD)]. The numbers indicate the $B(M1; \text{g.s.} \rightarrow 1^+)$ values (in μ_N^2) for transitions greater than 0.5 μ_N^2. Only states with $B(M1; g.s. \rightarrow 1^+)>0.1\ \mu_N^2$ are shown (solid lines: $B(M1)>0.3\ \mu_N^2$, dashed lines: $B(M1)<0.3\ \mu_N^2$). The upper portion shows the results obtained with standard pairing, Δ_{std}. The results obtained with pairing reduced by 50% are displayed in the lower portion. (From Ref. [34].)

high-j excitations, such as $(h_{11/2})^2$ or $(g_{9/2})^2$, has a simple shell model interpretation (in terms of a single-j shell) and cannot be viewed as coming from a collective "scissors" mode (see discussion in Ref. [35]). The synthetic orbital scissors state is defined as

$$|R\rangle = \mathcal{N}^{-1}\left(l_+^{(n)} - \alpha l_+^{(p)}\right)|\text{g.s.}\rangle\,, \tag{1}$$

where $\mathcal{N}$ is a normalization factor and the parameter α is determined by the requirement that the mode (1) is orthogonal to the spurious reorientation mode [33,36,37]. The calculations show that for the lowest 1^+ state in ^{76}Sr the overlap between its QRPA wave function and the state (1) is

only about 12%. Consequently, although this state is predicted to carry an unprecedented $M1$ strength, it cannot be given a geometric interpretation of the "scissors" mode. The $K^{\pi}=1^{+}$ isovector giant quadrupole resonance in ^{76}Sr lying at $E_{ex}\sim 32$ MeV carries a significant $M1$ strength ($\sim 4\ \mu_N^2$) and contains a major component of the "scissors mode" (around 50%).

When moving away from ^{76}Sr, the low-energy $M1$ strength becomes more fragmented. Good candidates to find large $M1$ strength at low energies are the well-deformed prolate nuclei ^{78}Sr, ^{80}Sr, ^{80}Zr, ^{82}Zr, and ^{74}Kr. The most promising oblate-shape candidate is the $N = Z$ nucleus ^{72}Kr. Similar to ^{76}Sr, the 1^{+} state in ^{72}Kr has a $(g_{9/2})^2$ character. However, in this case the main contribution comes from the high-Ω substates, *i.e.*, the π([413 7/2]$\otimes$[404 9/2]) and ν([413 7/2]$\otimes$[404 9/2]) configurations.

5. Summary

The present investigation has been focused on the microscopic structure of nuclei at particle drip lines. Predictions have been made about the nature and properties of yet unobserved structures. The most important observations can be summarized as follows:

(i) The self-consistent analysis based on the HF and RMF approaches indicates that there is a significant isospin dependence of spherical shell effects in medium-mass and heavy nuclei. The most interesting prediction is that the shell structure of neutron drip-line nuclei is dramatically affected by interaction with the continuum. Due to large diffuseness of neutron density and central potential, the single-particle spectrum of neutron-drip-line nuclei resembles that of the harmonic oscillator with the spin-orbit term. Clearly, the concept of nuclear surface and shape-deformations becomes rather weak for neutron-drip-line systems. Also, there are significant differences between predictions of HF and RMF models for isospin dependence of the neutron spin-orbit splitting.

(ii) The spectroscopy around the heaviest doubly-magic $N = Z$ nucleus ^{100}Sn has already become a reality. According to theoretical estimates, the proton binding energy of this nucleus should be around 3 MeV, and the Q_{EC} value – around 8 MeV.

(iii) In the N$\sim$Z nuclei from the light zirconium region there are many excellent candidates for the low-lying 1^{+} states with unusually large $B(M1; 0^{+} \rightarrow 1^{+})$ rates, around 1–2 μ_N^2. The best prospects are the Z=N nuclei, such as ^{76}Sr, ^{80}Zr, and ^{72}Kr, where protons and neutrons contribute equally strongly to the $M1$ collectivity. Interestingly, the unusually large low-energy $M1$ strength in those nuclei has a simple interpretation in terms of $(g_{9/2})^2$ excitations, *i.e.*, it does not result from a simplistic scissors mode.

Oak Ridge National Laboratory is managed for the U.S. Department of Energy by Martin Marietta Energy Systems, Inc. under contract No. DE-AC05-84OR21400. The Joint Institute for Heavy Ion Research has as member institutions the University of Tennessee, Vanderbilt University, and the Oak Ridge National Laboratory; it is supported by the members and by the Department of Energy through Contract No. DE-FG05-87ER40361 with the University of Tennessee. Theoretical nuclear physics research at the University of Tennessee is supported by the U.S. Department of Energy through Contract No. DE-FG05-93ER40770. This work was supported in part by the Polish State Committee for Scientific Research under Contract No. 204509101 and by the Swedish Research Council (NFR).

REFERENCES

[1] P. Möller, W.D. Myers, W.J. Świątecki, J. Treiner, *At. Data Nucl. Data Tables* **39**, 225 (1988).

[2] D. Hirata, H. Toki, T. Watabe, I. Tanihata, B.V. Carlson, *Phys. Rev.* **C44**, 1467 (1991).

[3] Y. Aboussir, J.M. Pearson, A.K. Dutta, F. Tondeur, *Nucl. Phys.* **A549**, 155 (1992).

[4] R. Smolańczuk, J. Dobaczewski, *Phys. Rev.* **C**, in press.

[5] P. Möller, J.R. Nix, W.D. Myers, W.J. Świątecki, *At. Data and Nucl. Data Tables*, to be published.

[6] J. Dobaczewski, I. Hamamoto, W. Nazarewicz, J.A. Sheikh, submitted for publication, 1993.

[7] M.M. Sharma, M.A. Nagarajan, P. Ring, *Phys. Lett.* **B312**, 377 (1993).

[8] J. Dobaczewski, H. Flocard, J. Treiner, *Nucl. Phys.* **A422**, 103 (1984).

[9] P. Ring, P. Schuck, *The Nuclear Many-Body Problem*, Springer-Verlag, 1980.

[10] G.A. Leander, J. Dudek, W. Nazarewicz, J.R. Nix, Ph. Quentin, *Phys. Rev.* **C30**, 416 (1984).

[11] J. Blomqvist, in Proceedings of the International Conference on Nuclei Far From Stability, Helsingør, CERN Report No. 81-09, 1981, p. 536.

[12] J. Dobaczewski, W. Nazarewicz, A. Płochocki, K. Rykaczewski, J. Żylicz, *Z. Phys.* **A329**, 267 (1988).

[13] A. Płochocki, K. Rykaczewski, T. Batsch, J. Szerypo, J. Żylicz, R. Barden, O. Klepper, E. Roeckl, D. Schardt, H. Gabelmann, P. Hill, H. Ravn, T. Thorsteinsen, I.S. Grant, H. Grawe, P. Manakos, L.D. Skouras, the ISOLDE Collaboration, *Z. Phys.* **A342**, 43 (1992).

[14] I. Hamamoto, H. Sagawa, *Phys. Rev.* **C48**, R960 (1993).

[15] J. Suhonen, T. Taigel, A. Faessler, *Nucl. Phys.* **A486**, 91 (1988).

[16] I.N. Borzov, E.L. Trykov, S.A. Fayans *Yad. Fiz.* **52**, 985 (1990); *Sov. J. Nucl. Phys.* **52**, 627 (1990).

[17] K. Ogawa, Contrib. 6th Intern. Conf. on Nuclei Far from Stability + 9th Intern. Conf. on Atomic Masses and Fundamental Constants, Bernkastel-Kues, Germany, 1992, p. E7.
[18] T. Nikolaus, T. Hoch, D.G. Madland, *Phys. Rev.* **C46**, 1757 (1992).
[19] L.D. Skouras, P. Manakos, *J. Phys.* **G19**, 731 (1993).
[20] T. Engeland, M. Hjort-Jensen, A. Holt, E. Osnes, *Phys. Rev.* **C48**, R535 (1993).
[21] C.J. Lister, B.J. Varley, H.G. Price, J.W. Olness, *Phys. Rev. Lett.* **49**, 308 (1982).
[22] H.G. Price, C.J. Lister, B.J. Varley, W. Gelletly, J.W. Olness, *Phys. Rev. Lett.* **51**, 1842 (1983).
[23] C.J. Lister, P.J. Ennis, A.A. Chishti, B.J. Varley, W. Gelletly, H.G. Price, A.N. James, *Phys. Rev.* **C42**, R1191 (1990).
[24] W. Nazarewicz, J. Dudek, R. Bengtsson, T. Bengtsson, I. Ragnarsson, *Nucl. Phys.* **A435**, 397 (1985).
[25] R. Bengtsson, in *Nuclear Structure of the Zirconium Region*, ed. by J. Eberth, R.A. Meyer and K. Sistemich, Springer-Verlag, 1988, p. 371.
[26] J.L. Wood, K. Heyde, W. Nazarewicz, M. Huyse, P. van Duppen, *Phys. Rep.* **215**, 101 (1992).
[27] W. Nazarewicz and T. Werner, in *Nuclear Structure of the Zirconium Region*, ed. by J. Eberth, R.A. Meyer and K. Sistemich, Springer-Verlag, 1988, p. 277.
[28] W. Ziegler, C. Rangacharyulu, A. Richter, C. Spieler, *Phys. Rev. Lett.* **65**, 2515 (1990).
[29] J. Margraf, R.D. Heil, U. Kneissl, U. Maier, H.H. Pitz, H. Friedrichs, S. Lindenstruth, B. Schlitt, C. Wesselborg, P. von Brentano, R.–D. Herzberg, A. Zilges, *Phys. Rev.* **C47**, 1474 (1993).
[30] D.R. Bés, R.A. Broglia, *Phys. Lett.* **137B**, 141 (1984).
[31] K. Heyde, C. de Coster, *Phys. Rev.* **44**, R2262 (1991).
[32] I. Hamamoto, C. Magnusson, *Phys. Lett.* **260B**, 6 (1991).
[33] I. Hamamoto, W. Nazarewicz, *Phys. Lett.* **297B**, 25 (1993).
[34] T. Nakatsukasa, K. Matsuyanagi, I. Hamamoto, W. Nazarewicz, submitted to *Nucl. Phys.* **A** (1993).
[35] I. Hamamoto, S. Åberg, *Phys. Lett.* **B145**, 163 (1984); *Phys. Scripta* **34**, 697 (1986).
[36] A. Faessler, R. Nojarov, *Phys. Rev.* **C41**, 1243 (1990).
[37] D. Zawischa, J. Speth, *Z. Phys.* **A339**, 97 (1991).